RSC Advances

PAPER

View Article Online
View Journal | View Issue

Cite this: *RSC Adv.*, 2022, **12**, 14819

Preparation and wide band emission characteristics of Eu^{2+}/Eu^{3+} co-doped $Ba_3P_4O_{13}$ phosphors

Wenke Ruan, Renrong Zhang, Qi Zhong, Yan Fu, Zhiwei Yang and Mubiao Xie*

Received 18th April 2022
Accepted 25th April 2022

DOI: 10.1039/d2ra02478k

rsc.li/rsc-advances

A series of phosphors $Ba_3P_4O_{13}$:$xEu^{2+/3+}$ (x = 0–0.1) were synthesized in a CO reduction atmosphere at a relatively low temperature (1113 K) by the solid-phase method. Crystallization and optical properties were investigated by using powder X-ray diffraction (XRD), X-ray photoelectron spectroscopy (XPS) and fluorescence spectrophotometry (PL/PLE), respectively. Under the excitation of 394 nm, the emission spectrum of the phosphor presents a broad spectrum band of Eu^{2+} and characteristic peaks of Eu^{3+} in the range of 400–750 nm, indicating the coexistence of Eu^{2+} and Eu^{3+} in the system. The occupation of Eu^{2+} and Eu^{3+} in the $Ba_3P_4O_{13}$ matrix position was discussed by Gaussian fitting and PL spectra. The existence of energy transfer between Eu^{2+} → Eu^{3+} in the system can be found through PL spectra under excitation of 251 nm. The emission color of the phosphor can be adjusted by changing the Eu ion doping concentration, resulting in the CIE color coordinates changing from (0.213, 0.215) blue to (0.249, 0.261) light bluish white. The results show that $Ba_3P_4O_{13}$:$Eu^{2+/3+}$ phosphors can be used as a potential single-doped single-host white light-emitting material.

Introduction

White light-emitting diodes (w-LEDs) are gradually becoming a new generation of green light sources due to their outstanding advantages such as small size, environmental protection, energy saving, high efficiency, and long life. They have been widely used in various fields such as lighting, display, communication, medical treatment, and biological applications.[1–4] At present, commercial w-LEDs are mainly packaged by a combination of blue chips (GaInN) and yellow phosphors (YAG:Ce^{3+}/red-green sulfide phosphors) or blue chips (GaInN) and three-primary phosphors. However, this type of device practically results in a low rendering index and high color temperature due to the lack of red phosphor components, which makes it far from the best requirements in the mass market.[5–7] Therefore, it is desired to use ultraviolet LED chips and single-doped single matrix white light phosphors to prepare w-LEDs to solve the above problems. It is because that ultraviolet light has higher energy and does not participate in the white light composition, color control is easier, and it can also avoid excessive the re-absorption of blue and red light, coupled with the simple packaging process, has become a research hotspot in recent years.

At present, the active ions doped with single matrix white phosphors mainly include:[8–11] Dy^{3+}, Ce^{3+}/Eu^{2+}, Mn^{2+}/Eu^{2+}, Eu^{2+}/Eu^{3+}, *etc.* Among them, Eu^{2+}/Eu^{3+} have different energy level structures.[12–14] Eu^{3+} ions are subject to the f–f transition forbidden and can produce orange-red light characteristic narrow linear spectrum.[15] However, there are shortcomings such as low display index, luminous efficiency and weak spectral line intensity. The electronic transition of Eu^{2+} belongs to the allowable transition of 4f–5d spin, it is easily affected by the coordination environment due to the orbital is exposed. It can effectively absorb ultraviolet light and can produce high-intensity broad peaks. More importantly, depending on the structure of the matrix, it emits various spectra from blue to red.[16] Eu^{2+} and Eu^{3+} coexist in the fluorescent matrix which to improve the luminous performance of the phosphor *via* the different optical properties of the two can be used at the same time, and even a single matrix white phosphor can be obtained.[17,18]

Generally, the matrix is also an important component of the luminescent material. In many matrix systems, phosphate matrix is one of the representatives. Among them, the phosphate $Ba_3P_4O_{13}$ has the advantages of low preparation cost, relatively simple technical process, low synthesis temperature, good stability, and low cost.[19–28] In recent years, it has become more and more popular among scientific researchers. As early as 1986, Millet *et al.*[19] reported that $Ba_3P_4O_{13}$ phosphate single crystal has a low-temperature phase and a high-temperature phase, and its transition temperature is 870 °C. In 1991, Gatehouse *et al.*[20] reported the crystal structure of $Ba_3P_4O_{13}$, which the low temperature phase belongs to the triclinic system and the high temperature phase belongs to the orthorhombic system. In 2002, Bennazha *et al.*[21] studied the distribution of atoms in the low-temperature phase $Ba_3P_4O_{13}$ crystal system and there are four different Ba^{2+} lattice sites in the system. In

School of Chemistry and Chemical Engineering, Lingnan Normal University, Zhanjiang 524048, China. E-mail: xiemubiao@163.com

2013, Zhang *et al.*[22] synthesized $Ba_3P_4O_{13}$:Eu^{2+} phosphor by a high-temperature solid-phase method, and used a charge compensation mechanism to explain that Eu^{3+} ions can also be reduced to Eu^{2+} ions at high temperature in an air atmosphere. In 2015, Guo *et al.*[23] synthesized a new type of $Ba_3P_4O_{13}$:Eu^{2+} long-lasting phosphor by solid-phase method and studied the optical properties. In 2016, Li *et al.*[24] synthesized high-temperature $Ba_3P_4O_{13}$:Eu^{2+} yellow phosphor by high-temperature solid-phase method, and studied the energy transfer between Eu^{2+} occupying different positions of Ba^{2+} and Eu^{2+}. In 2017, Wu *et al.*[25] reported a tunable full-color luminescent $Ba_3P_4O_{13}$:Eu^{2+} phosphor and the $Ba_3P_4O_{13}$ was transformed from a low-temperature phase form to a high-temperature phase form through different Eu^{2+} doping concentrations, emitting blue and yellow light respectively. The change is closely related to the specific crystal phase structure of the main body. Recently, Wu *et al.*[26] used La^+ and Na^+ to replace the Ba^{2+} cations in the $Ba_3P_4O_{13}$ matrix based on the original research, and realized the color change of $Ba_{2.94-2x}La_xNa_xP_4O_{13}$:0.06Eu phosphor from blue–green–white–orange. In 2019, Du *et al.*[27] synthesized $Ba_3P_4O_{13}$:Eu^{3+} red phosphor by sol–gel, which analyzed Eu^{3+} ions in the host lattice of the local crystal environment around $Ba_3P_4O_{13}$, and it is confirm that the good thermal stability of the phosphor through temperature control. In 2021, Yan *et al.*[28] synthesized a new type of single-phase $Ba_3P_4O_{13}$:Dy^{3+}, Eu^{3+} phosphor by co-precipitation method. The energy transfer from Dy^{3+} to Eu^{3+} has an efficiency of 38.97%, by adjusting the content of Eu^{3+} or the excitation wavelength, the spectrum emission from cool white to yellowish white is realized. It is a promising single-component white light luminescent material. As mentioned above, through different preparation methods, different activation ions, and activation ions occupying different coordination environments, *etc.*, the luminescence performance of the phosphor can be effectively adjusted, and the white light emission of the LED with a single doping and single composition can be achieved.

In this paper, the pure phase $Ba_3P_4O_{13}$:Eu^{2+}/Eu^{3+} phosphor was synthesized under the CO reduction atmosphere by solid-phase method. The crystal structure, excitation and emission spectra of the sample were studied, combined with the analysis of the different coordination of Eu ions occupying Ba^{2+} in the matrix, which to analyze the cause of the asymmetry of the emission spectra. Under the CO reduction atmosphere, Eu^{2+} and Eu^{3+} coexist in the $Ba_3P_4O_{13}$ system. In this system, there is energy transfer between Eu^{2+} and Eu^{3+}, which can be effectively excited in the range of 250–400 nm ultraviolet light, achieving tunable emission from blue to light bluish white. Studies have shown that $Ba_3P_4O_{13}$:$Eu^{2+/3+}$ can be used as a single-doped single-host white light-emitting material with potential application prospects.

Experimental section

Synthesis of $Ba_3P_4O_{13}$:$Eu^{2+/3+}$

Series phosphors $Ba_3P_4O_{13}$:$xEu^{2+/3+}$ ($x = 0$–0.1) were prepared by high-temperature solid-phase method. The raw materials were barium carbonate (Ba_3CO_3, AR), ammonium dihydrogen phosphate ($NH_4H_2PO_4$, AR) and europium oxide (Eu_2O_3, 99.99%). According to the stoichiometric ratio $Ba_3P_4O_{13}$: xEu (x = 0, 0.01, 0.02, 0.04, 0.06, 0.08, 0.1), calculate the amount of raw materials needed, weigh, mix thoroughly, grind evenly, and then load the ground samples into corundum In the crucible. With the corundum crucible containing the raw materials in a high-temperature box-type resistance furnace, calcined at 1113 K for 4 hours under CO atmosphere reduction conditions, and naturally cool to room temperature to obtain $Ba_3P_4O_{13}$:xEu (x = 0–0.1) series phosphors.

Characterization of the $Ba_3P_4O_{13}$:$Eu^{2+/3+}$

Use Bruker AXS D8 advance X-ray diffractometer (XRD) to test the phase composition of the sample. The radiation source is Cukα rays. Test conditions: tube voltage 40 kV, tube current 40 mA, scanning range 10–80°; the morphology and energy spectrum were analyzed through Thermal field emission Scanning Electron Microscope (FESEM, JSM-7610F) under an acceleration voltage of 11 kV, and energy disperse spectroscopy (EDS, NORAN System7), respectively; X-ray photoelectron spectroscopy (XPS) analysis was carried out on a ThermoFischer, ESCALAB Xi+ spectrometer using the monochromatic Al Kα excitation source (1486.6 eV). The excitation, emission spectra and fluorescence lifetime of the samples were measured with the FLS1000 steady-state transient fluorescence spectrometer from Edinburgh, UK. The 450 w of xenon lamp was used as the excitation source, and the excitation and emission slits were 0.2–1 nm. All tests are performed at room temperature.

Results and discussion

Fig. 1 shows the X-ray diffraction pattern (XRD) of the samples $Ba_3P_4O_{13}$:xEu (x = 0.005, 0.01 and 0.1). The compound $Ba_3P_4O_{13}$ has two crystal structures, the low temperature phase (JCPDS 36-1489) and the high temperature phase (JCPDS 12-0689).[19] As shown in Fig. 1, the diffraction peaks of the synthesized sample are basically the same as the standard card JCPDS 36-1489. It is shows that the synthesized $Ba_3P_4O_{13}$ samples are the target products of the low-temperature phase. Some impurities with minor peaks are identified as (*BaO_2 (JCPDS#07-0233) and

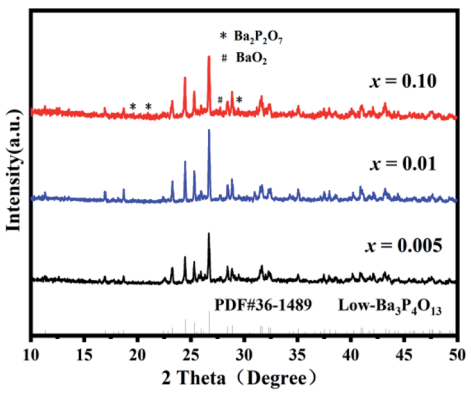

Fig. 1 XRD patterns of $Ba_3P_4O_{13}$ doped with different Eu ion concentrations.

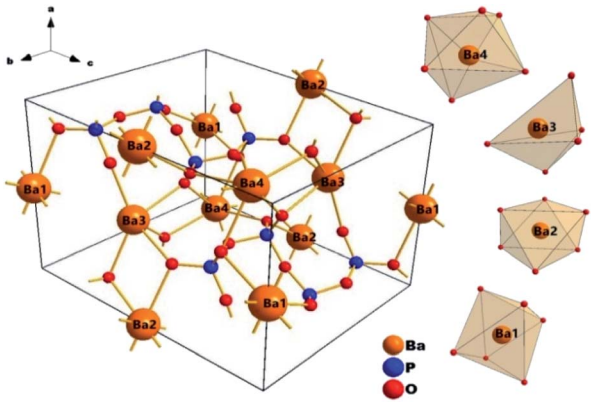

Fig. 2 $Ba_3P_4O_{13}$ unit-cell crystal structure diagram and the coordination environment of the polyhedron [Ba(1)O6], [Ba(2)O6], [Ba(3)O5], and [Ba(4)O7].

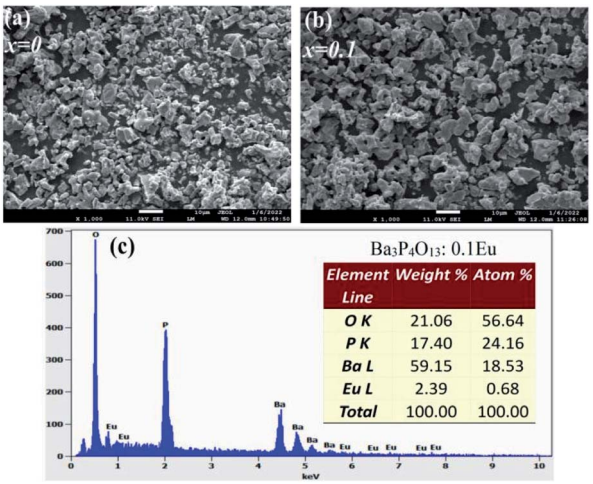

Fig. 3 The FESEM images of $Ba_3P_4O_{13}$:xEu (x = 0, 0.1) (a and b), and the corresponding EDS measurements with the element ratios (c).

#$Ba_2P_2O_7$ (JCPDS#30-0144)), which may be caused by insufficient precursor reaction and a small quantity of phase change won't significantly affect our analysis. All in all, the small amount of $Eu^{2+/3+}$ ions doping into $Ba_3P_4O_{13}$ does not cause the change of the crystal structure.

The low-temperature phase $Ba_3P_4O_{13}$ belongs to the triclinic system, the space group is $P1$ or $P(-1)$, and the unit cell parameters are a = 5.691(5), b = 7.238(7), c = 8.006(5) Å, α = 83.65 (5), β = 75.95(8), γ = 70.49(7).[20] Its unit-cell crystal structure is shown in Fig. 2. On the basis of the Wyckoff principle, there are 4 different Ba^{2+} positions in the $Ba_3P_4O_{13}$ structure, namely Ba(i) (i = 1,2,3,4), Ba(1), Ba(2), Ba(3) and Ba(4). As a result of the electrical neutrality, when Eu^{3+} replaces Ba^{2+}, the four Ba^{2+} lattice sites cannot be completely occupied, which to change the bond angle and bond length. According to three different chemical bond positions, it can be known that the four of Ba^{2+} positions are distributed in the three groups. Two calcium sites (Ba(1) and Ba(2)) are coordinated by 6 oxygen atoms, while the other cation sites are coordinated by 5(Ba(1)) oxygen atoms and coordinated by 7(Ba(4)) oxygen atoms respectively. Therefore, Ba(Eu) is in a chemical environment with 5, 6 and 7 coordination numbers. Since the ionic radius of Eu^{2+} and Eu^{3+} is similar to that of Ba^{2+} in the matrix, it can be inferred that Eu also comes from different the luminescent center, which shows that Eu^{2+} and Eu^{3+} doping will occupy two or more different positions of Ba^{2+}.

Fig. 3(a and b) show the SEM image of the $Ba_3P_4O_{13}$:xEu (x = 0, 0.1) phosphor. The studied samples are composed of irregular and agglomerated particles with an average size of 1–10 μm, which the addition of Eu ions makes the agglomeration more obvious. In order to further clarify the element composition of the synthesized sample. Fig. 3(c) shows the EDS measurements of $Ba_3P_4O_{13}$:0.1Eu phosphor, all the elements (Ba, P, O and Eu) of $Ba_3P_4O_{13}$:0.1Eu can be detected, which further confirms that the expected sample has been synthesized success.

Fig. 4a exhibits XPS survey scan of the $Ba_3P_4O_{13}$:0.08Eu (Eu^{2+}, Eu^{3+}) prepared in the CO reducing atmosphere. The total survey results (Fig. 4a) indicate the elements of Ba, P, O and Eu, respectively, affirming chemical composition of the title phosphor. To confirm the different types of Eu ions, Fig. 4b depicts high-resolution spectra of Eu-3d of in the samples, and both Eu^{2+} and Eu^{3+} signals ascribed to $3d_{5/2}$ and $3d_{3/2}$ are observed.

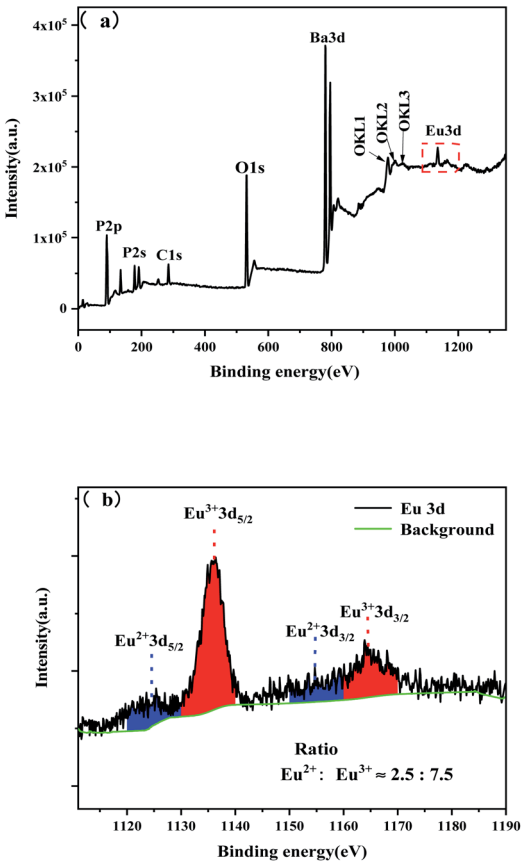

Fig. 4 XPS survey spectrum of $Ba_3P_4O_{13}$:0.8Eu (Eu^{2+}, Eu^{3+}) (a) and (b) high-resolution spectra of Eu 3d core level in $Ba_3P_4O_{13}$:0.8Eu (Eu^{2+}, Eu^{3+})

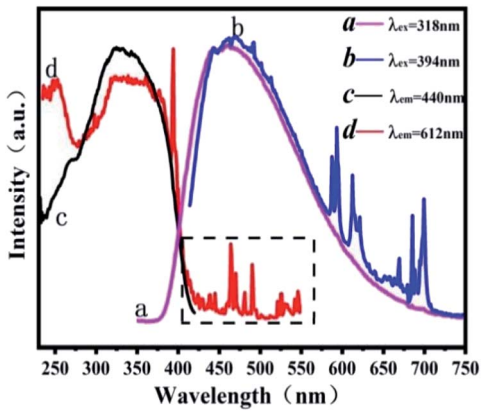

Fig. 5 Photoluminescence excitation (λ_{em} = 440, 612 nm) and emission (λ_{ex} = 318, 394 nm) spectra of $Ba_3P_4O_{13}$:0.08$Eu^{2+/3+}$.

More importantly, the coexistence ratio of Eu^{2+} and Eu^{3+} was revealed to be approximately 2.5 : 7.5.

Fig. 5 shows the excitation and emission spectra of the sample $Ba_3P_4O_{13}$:0.08$Eu^{2+/3+}$ phosphor. The emission spectrum under the excitation of 318 nm ultraviolet light is shown in Fig. 5(a). It can be clearly seen that the emission spectrum is composed of an asymmetric and extremely wide single peak, which extends from the near ultraviolet region of 375 nm to the red region of 700 nm. The peak is at 461 nm, which belongs to Eu^{2+} of $4f^65d^1 \rightarrow 4f^7$ transition.

The emission spectrum under the excitation of 394 nm ultraviolet light is shown in Fig. 5(b). The emission spectrum is composed of a broad spectral band and a series of linear spectral bands, among which the broadband emission at 410–750 nm belongs to the 5d → 4f transition of Eu^{2+}. In the emission spectrum, a series of linear emission originates from the unreduced Eu^{3+} luminescence center, which is located at 587, 593, 612 and 699 nm from the $^5D_0 \rightarrow {}^7F_j$ (j = 0–4) characteristic transition of Eu^{3+}, respectively. It can be seen that Eu^{3+} can be partially reduced to Eu^{2+} in a reducing atmosphere, while Eu^{3+} and Eu^{2+} coexist in the synthesized sample. It can be seen from Fig. 5(b) that the intensity is highest at $^5D_0 \rightarrow {}^7F_1$(593 nm), followed by $^5D_0 \rightarrow {}^7F_2$(612 nm), indicating that the magnetic dipole transition ($^5D_0 \rightarrow {}^7F_1$) is dominant and Eu^{3+} occupies the center of inversion symmetry. In other words, Eu^{3+} will occupy a position with higher symmetry.

The excitation spectrum monitored at 440 nm is shown in Fig. 5(c). The excitation spectrum 230–420 nm consists of a small broad spectral band and a large broad spectral band, with peaks at 273 nm and 325 nm, respectively. At the same time, there is a shoulder peak hidden at 375 nm, and all excitation bands belong to the transition from the $4f^7(^8S_{7/2})$ ground state of Eu^{2+} to the excited state $4f^65d^1(^7F)$. Since the 5d orbital of Eu^{2+} is in a bare environment, it is particularly susceptible to splitting two broad peaks under the influence of the crystal field. The two broad peaks also appear in this article, indicating that Europium ions have at least two different luminescence centers, which also confirms Ba^{2+} has different cation positions.

The excitation spectrum monitored at 612 nm is shown in Fig. 5(d). The excitation spectrum ranges from 230 to 550 nm and consists of two broad bands and a series of small excitation peaks. Among them, the charge transfer band (CTB) of $O^{2-} \rightarrow Eu^{3+}$ at 230–270 nm. It is formed by the overlap of the charge transfer band of $O^{2-} \rightarrow P^{5+}$ with a broad absorption peak at 270–390 nm centered at 325 nm, while a series of small excitation peaks appearing in the range of 390–550 nm are derived from the f → f transition of the higher energy level of Eu^{3+}. Among them, three strong excitation peaks can be observed at 394 nm, 465 nm and 528 nm, which are attributed to the characteristic transitions of $^7F_0 \rightarrow {}^5L_6$, $^7F_0 \rightarrow {}^5D_2$ and $^7F_0 \rightarrow {}^5D_1$, separately. It means the $Ba_3P_4O_{13}$:0.08$Eu^{2+/3+}$ phosphor can be effectively excited by the ultraviolet light chip and the blue light chip, which is of great significance for white light LED lighting.

In addition, it can be clearly seen from Fig. 5 that the excitation spectrum of Eu^{3+} (λ_{em} = 612 nm) has a spectral absorption band ranging from 230 to 550 nm (as shown in Fig. 3d), and a strong overlap with the emission spectrum (λ_{ex} = 318 nm) of Eu^{2+}, which an emission band ranging from 350 to 700 nm (as shown in Fig. 5a). Therefore, it can be preliminarily inferred that there may be energy transfer between Eu^{2+} and Eu^{3+}.

In order to further analyze the influence of the concentration of the activator on the luminescence characteristics of the phosphor. Fig. 6 shows the emission spectrum samples of

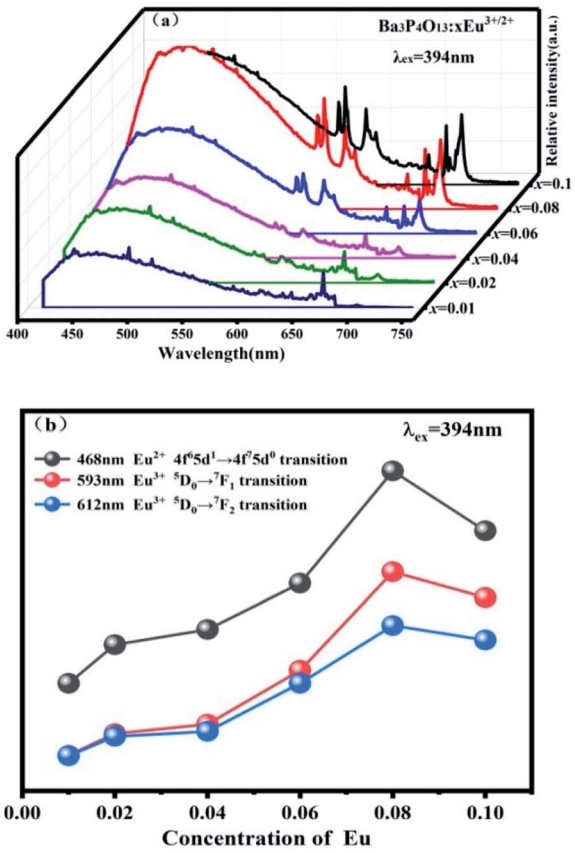

Fig. 6 The emission spectrum of $Ba_3P_4O_{13}$:xEu (x = 0–0.1) phosphor under excitation at 394 nm (a) and the emission intensity with peaks at 468 nm, 593 nm and 612 nm as a function of Eu ion concentration (b).

$Ba_3P_4O_{13}$:xEu (x = 0–0.1) series phosphors excited by 394 nm ultraviolet light. It can be seen from Fig. 6(a) that when the europium (Eu) ion concentration is low, the Eu^{2+} characteristic emission peak appears more obvious, while the Eu^{3+} characteristic emission peak hardly appears. As the rare earth europium (Eu) ion doping the impurity concentration increases, the characteristic emission peak of Eu^{3+} becomes more and more obvious. It is shows that when the concentration of doped europium (Eu) ions is low, the trivalent europium (Eu) ions are reduced relatively completely, which the valence state of Eu ions is stable at divalent. With the increase of doping concentration, trivalent Eu ions gradually appeared in the system, the excessive trivalent Eu ions could not be completely reduced to divalent Eu ions, resulting in the coexistence of Eu^{2+} and Eu^{3+} in the system. Furthermore, as the europium (Eu) ion concentration increases, the luminous intensity of the characteristic emission peaks of Eu^{2+} and Eu^{3+} both increase first and then decrease, reaching the maximum when the europium ion concentration $x = 0.08$, as shown in Fig. 6(b). On the one hand, with the concentration of europium ions increases, it promotes the $Eu^{3+} \rightarrow Eu^{2+}$ reduction reaction. The number of Eu^{2+} luminescence centers is increasing rapidly, while the number of Eu^{3+} luminescence centers is also gradually increasing, and the luminescence is continuously enhanced. On the other hand, when the Eu^{2+} and Eu^{3+} ion concentration reaches a certain critical value, the distance between the luminescent centers gradually decreases, resulting in an increase in the probability of non-radiative transition between ions. It means that more energy is released in a non-radiative relaxation manner, which leads to the quenching of the luminous concentration and the reduction of the emitted light intensity. The concentration quenching effect originates from the non-radiative energy transfer between ions, and the non-radiative energy transfer has two forms: exchange interaction and multipolar interaction. The type of interaction can be determined by analyzing the mechanism of concentration quenching. Blasse[29] pointed out that the critical distance Rc for quenching the luminous ion concentration can be obtained by formula (1):

$$R_c = 2\left(\frac{3V}{4\pi X_c N}\right)^{1/3} \quad (1)$$

In the formula, V is the unit cell volume, X_c is the quenching concentration, and N is the number of cations in the unit cell that can be replaced by activator ions. According to the literature 21 $Ba_3P_4O_{13}$ unit cell volume V = 600.65 Å^3. For $Ba_3P_4O_{13}$:xEu (x = 0–0.1) phosphor, N = 2, X_c = 0.08, the critical distance R_c = 19.38 Å is estimated. Blasse[29] believes that if R_c is greater than 5 Å, the electric multipole moment interaction is the concentration quenching mechanism, otherwise it is the electron cloud exchange. In this system, R_c is much larger than 5 Å, so the concentration quenching mechanism is the electric multipole moment interaction.

As shown in Fig. 7, the emission peak of $Ba_3P_4O_{13}$:xEu(x = 0–0.1) phosphor under excitation at 251 nm was monitored. It can be seen from Fig. 7(a) that the emission spectrum under excitation at 251 nm is basically similar to the emission spectrum under excitation at 394 nm in Fig. 7. When the europium ion concentration $x \leq 0.08$, with the increase of the concentration, the characteristic emission peaks of Eu^{2+} and Eu^{3+} become stronger and stronger. When the europium ion concentration $x > 0.08$, the $4f^65d^1 \rightarrow 4f^7d^0$ characteristic peak intensity of Eu^{2+} decreases rapidly, however, the $^5D_0 \rightarrow {}^7F_1$ and $^5D_0 \rightarrow {}^7F_2$ characteristic peak intensity of Eu^{3+} is still increasing, as shown in Fig. 7(b). As described in Fig. 3 above, there is a significant overlap between the emission energy level of Eu^{2+} and the excitation energy level of Eu^{3+}, that is, Eu^{2+} can

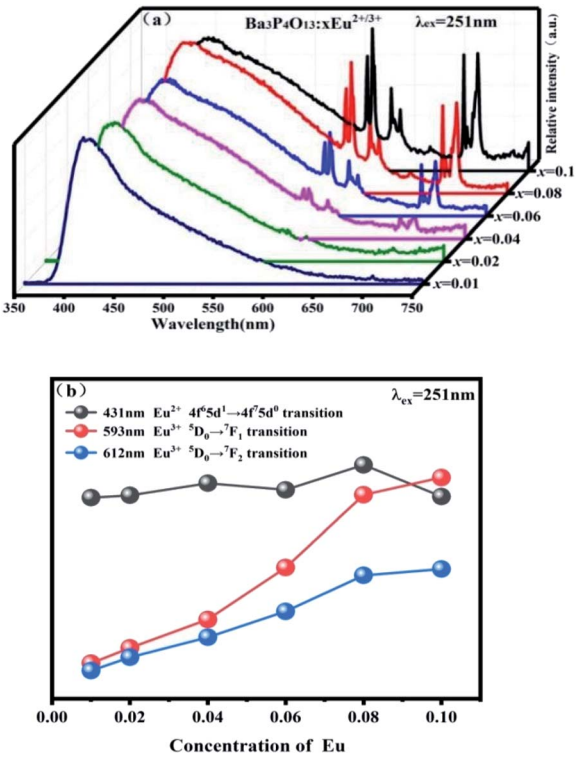

Fig. 7 The emission spectrum of $Ba_3P_4O_{13}$:xEu (x = 0–0.1) phosphor under excitation at 251 nm (a) and the emission intensity with peaks at 431 nm, 593 nm and 612 nm as a function of Eu ion concentration (b).

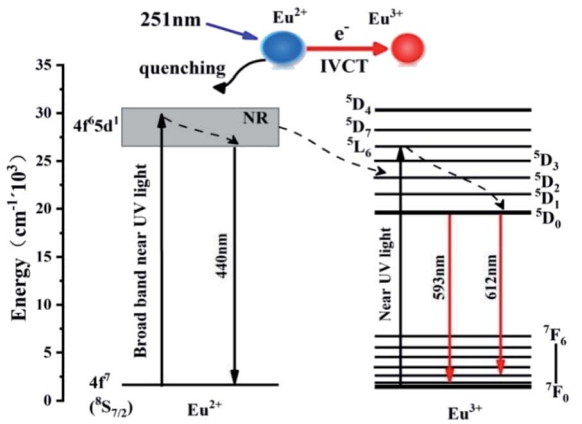

Fig. 8 Energy level diagram of Eu^{2+} and Eu^{3+} in $Ba_3P_4O_{13}$ matrix.

effectively sensitize Eu^{3+}. As shown in Fig. 8, under the excitation of 251 nm light, the electrons of Eu^{2+} in the ground state of $^8S_{7/2}$ are excited and transition to the $4f^65d^1$ energy level, and part of the electrons in the excited state returns to the ground state energy level by means of radiation transition, and the other part transitions to the $^5D_2$ energy level of Eu^{3+} by means of energy transfer, and then radiates the transition back to the $7F_0$ ground state energy level.

Fig. 9 demonstrates the normalized photoluminescence emission (PL) spectra of the sample $Ba_3P_4O_{13}$:xEu (x = 0–0.1) series phosphors excited by 251 nm and 318 nm ultraviolet light. With the increase of Eu ion doping concentration, the Eu^{2+} characteristic emission spectrum peak of Fig. 9(a) red-shifts from 416 nm to 431 nm, and that in Fig. 9(b) red-shifts from 435 nm to 460 nm, which may be caused by the crystal field splitting where Eu^{2+} is located. Furthermore, it can be seen from Fig. 9 that under different excitation wavelengths, two different emission spectra appear, the excitation at a wavelength of 251 nm, the emission spectrum simultaneously appears Eu^{2+} and Eu^{3+} characteristic emission, while under 318 nm wavelength excitation, there is only Eu^{2+} characteristic emission. As the excitation wavelength increases from 251 nm to 318 nm, the Eu^{2+} characteristic broad peak has a significant red shift, and the broad peak emission peak shifts from 433 nm to 460 nm. This indicates that $Eu^{2+/3+}$ occupies at least two different lattice sites in the $Ba_3P_4O_{13}$ matrix. It was confirmed with Bennzha *et al.*[21] that there are four independent Ba^{2+} sites in the low-temperature phase $Ba_3P_4O_{13}$ unit cell, which are very suitable for $Eu^{2+/3+}$ to be occupied.

Many studies have shown that the valence state and size effect are the two key factors that determine the dopant occupancy in the crystal. It is generally believed that ions with the same valence state and similar radii are more likely to occupy the ions in the matrix.[30] As shown in Table 1, the valence states of Eu^{2+} and Ba^{2+} are the same, and the radius is similar, which shows that Eu^{2+} replaces the Ba^{2+} position more preferentially than Eu^{3+}. Therefore, in order to discuss the position occupancy of $Eu^{2+/3+}$ in the matrix, Gaussian peak separation processing was performed on the emission spectrum of the sample. Fig. 10(a) shows the emission spectrum and Gaussian peak fitting curve of $Ba_3P_4O_{13}$:0.08$Eu^{2+/3+}$ excited by 318 nm ultraviolet light. It can be seen that the emission spectrum of the sample can be decomposed into four Gaussian peaks with a higher degree of fit, which the peaks are located at 420 nm, 448 nm, 489 nm and 547 nm, and the corresponding excitation spectra are shown in Fig. 10(b). It can be seen from Fig. 10(b) that located at the three emission bands of 448 nm, 489 nm and 547 nm, which the excitation spectra have a slight difference in peak position and intensity, and the peak shapes are roughly the same. They are all composed of an asymmetric broadband single peak. However, the excitation spectrum of the 420 nm emission band has two broad peaks, which are quite different from the peak shapes of the first three, which indicates that $Eu^{2+/3+}$ may occupy multiple different Ba^{2+} sites in the $Ba_3P_4O_{13}$

Table 1 $Ba_3P_4O_{13}$:$Eu^{2+/3+}$ each ion radius[22,30]

Ion	Eu^{2+}		Eu^{3+}		Ba^{2+}		P^{5+}	O^{2-}
Ligancy	6	7	6	7	6	7	6	6
Radius/(10^{-10} m)	1.17	1.20	0.95	1.01	1.36	1.38	0.38	1.40

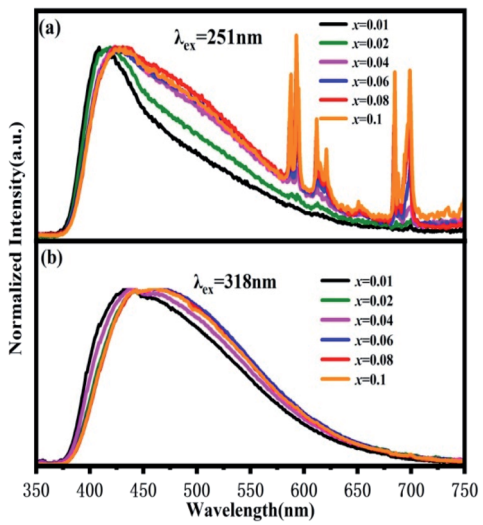

Fig. 9 Normalized PL spectra of $Ba_3P_4O_{13}$:xEu (x = 0–0.1) phosphor under excitation at 251 nm (a) and 318 nm(b).

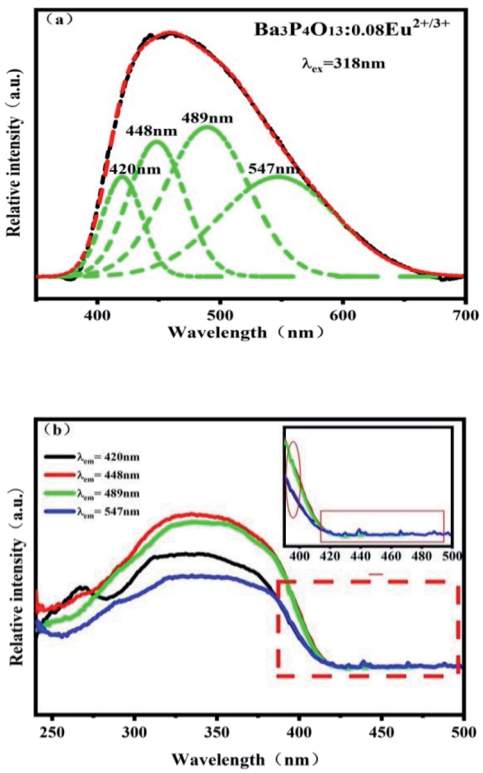

Fig. 10 $Ba_3P_4O_{13}$:0.08Eu emission spectrum and Gaussian fitting results (a) and excitation spectra (monitoring wavelength λ_{em} = 420 nm, 448 nm, 489 nm and 547 nm) under excitation at 318 nm (b).

matrix. Since the excitation spectrum of the 420 nm emission band is different from the other three peak types, it is preliminarily speculated that the emission band of 420 nm mainly comes from the Eu^{2+} luminescence center occupying 5 O atoms coordinated Ba(3) sites, while the other three emission bands are derived from Eu^{2+} luminescence centers that occupy 6 and 7 O atoms coordinated Ba(1), Ba(2) and Ba(4) sites. As the crystal field environment is similar to the coordination number, the shorter the Eu^{2+}–O^{2-} average bond length, the greater the field strength of the crystal field, and the longer the Eu^{2+} emission wavelength.[31] Therefore, it is speculated that the emission bands of 448 nm, 489 nm and 547 nm come from the Eu^{2+} luminescence centers on the Ba(2), Ba(1) and Ba(4) lattice sites, respectively. In addition, it can be seen from the inset of Fig. 10(b) that there are relatively weak Eu^{3+} characteristic peaks in the range of 390–500 nm, indicating that Ba(1), Ba(2), Ba(3) lattice sites and Ba(4), the position is also slightly occupied by Eu^{3+}. If considering their more specific occupation, it still needs further discussion in the future.

Fig. 11 shows the emission spectra of $Ba_3P_4O_{13}$:0.08Eu at different excitation wavelengths (λ_{ex} = 251–394 nm) and the corresponding CIE color coordinates. It can be seen from Fig. 11(a) that when the excitation wavelength increases from 251 nm to 260 nm, the intensity of blue and red light increases accordingly. When the excitation wavelength increases from 318 nm to 381 nm, only blue light appears and its intensity gradually decreases. However, as the excitation wavelength increases to 394 nm, blue and red light appear at the same time. It can be seen from Fig. 11(b) that when the excitation wavelength increases from 251 nm to 394 nm, the CIE color coordinate of the phosphor changes from (0.240, 0.261) to (0.244, 0.293), which the light-emitting color changes from light blue-white to blue color, back to light blue and white.

Fig. 12 shows the corresponding CIE color coordinates of $Ba_3P_4O_{13}$:xEu(x = 0–0.1) series phosphors excited by 251 nm ultraviolet light. It can be seen from Fig. 12 that as the Eu ion doping concentration increases, the light emission color changes from blue to light bluish white. By controlling the doping concentration of Eu ions, the color change of the phosphor can be appropriately adjusted, indicating that $Ba_3P_4O_{13}$:$Eu^{2+/3+}$ can be considered as a potential single-doped single-matrix white phosphor material. Compared with the $Ba_{2.94-2x}La_xNa_xP_4O_{13}$:0.06Eu synthesized by Wu *et al.*[26] and the $Ba_3P_4O_{13}$:Dy^{3+}, Eu^{3+} phosphor synthesized by Yan *et al.*[28] In this study, the $Ba_3P_4O_{13}$:Eu^{2+}/Eu^{3+} phosphor system not only does not add charge compensator and other different activating ions, but also can emit blue and red light at the same time in the 400–750 nm region. The results indicated that color-tunable white light emission is successfully achieved and optimized in single phase $Ba_3P_4O_{13}$:$Eu^{2+/3+}$ host, which enables the $Ba_3P_4O_{13}$:$Eu^{2+/3+}$ phosphors to be potential color-tunable phosphor candidates for WLEDs.

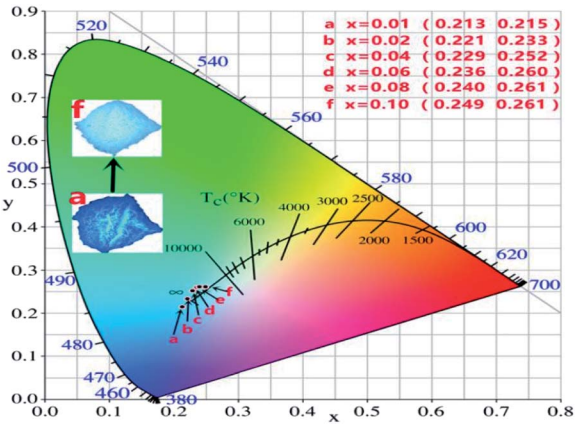

Fig. 12 CIE chromaticity coordinates of $Ba_3P_4O_{13}$:xEu (x = 0–0.1) phosphors. The digital images of the phosphors under 365 nm excitation are shown in the inset.

Conclusions

The Eu^{2+}/Eu^{3+} coexisting $Ba_3P_4O_{13}$:xEu(x = 0–0.1) series phosphors were synthesized by solid-phase method in a relatively low temperature (1113 K) CO reduction atmosphere. The phosphor can be effectively excited by ultraviolet light between 250 and 400 nm. Under excitation at 251 and 394 nm, the emission spectrum is composed of a wider spectral band in the blue region and a series of linear spectral bands in the red region, respectively. The superposition of the two bands shows blue-white light emission, and there is energy transfer between Eu^{2+} → Eu^{3+} in the system. Under 318 nm excitation, the emission spectrum consists of an asymmetric broad peak, which mainly emits blue light, and four emission peaks with peaks of 420 nm, 448 nm, 489 nm and 547 nm are obtained by Gaussian fitting, which verifies that Eu^{2+} and Eu^{3+} occupy four different Ba^{2+} sites in the $Ba_3P_4O_{13}$ matrix. Through changing the doping concentration of Eu ion to obtain a phosphor with adjustable color, the optimal doping concentration of $Eu^{2+/3+}$ is 0.08, and the CIE color coordinate can be obtained from (0.213, 0.215) blue to (0.249, 0.261) light bluish white adjustable emission. The above research results show that $Ba_3P_4O_{13}$:$Eu^{2+/3+}$ phosphor can provide a reference for the development of single-doped single-host white light-emitting materials.

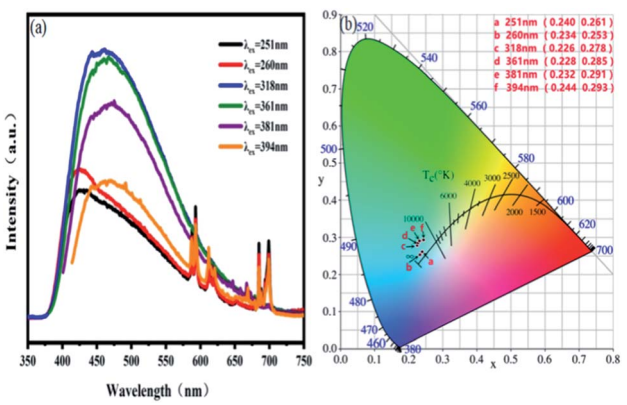

Fig. 11 $Ba_3P_4O_{13}$:0.08Eu emission spectrum (a) and color coordinate diagram (b) under excitation at different wavelengths (λ_{ex} = 251 nm, 260 nm, 318 nm, 361 nm, 381 nm and 394 nm).

Conflicts of interest

There are no conflicts to declare.

Acknowledgements

The work is financially supported by Guangdong Basic and Applied Basic Research Foundation (2022A1515011586), Research Group of Rare Earth Resource Exploiting and Luminescent Materials (2017KCXTD022).

References

1 B. Q. Shen, B. J. Chen, Y. P. Zhang and J. X. Hu, *J. Lumin.*, 2020, **218**, 116821.
2 F. Xu, L. Z. Fang, X. Zhou, H. P. Xia, J. L. Zhang, H. W. Song and B. J. Chen, *Opt. Mater.*, 2020, **108**, 110222.
3 X. L. Wang, S. L. Zhao, Y. J. Zhang and G. D. Sheng, *J. Rare Earths*, 2010, **28**, 222–224.
4 X. Yang, Y. Zhang, X. J. Zhang, J. Chen, H. S. Huang, D. S. Wang, X. R. Chai, G. N. Xie, M. S. Molokeev, H. R. Zhang, Y. L. Liu and B. F. Lei, *J. Am. Ceram. Soc.*, 2019, **103**, 16858.
5 S. J. Yu, Q. Chen, Y. Z. Lu, B. Q. Cao, J. K. Li and Z. M. Liu, *Opt. Mater.*, 2020, **111**, 110566.
6 P. Muralimanohar, G. Srilatha, K. Sathyamoorthy, P. Vinothkumar, M. Mohapatra and P. Murugasen, *Optik*, 2020, **225**, 165807.
7 M. F. Xia, Z. H. Ju, H. Yang, Z. B. Wang, X. P. Gao, F. X. Pan and W. S. Liu, *J. Alloys Compd.*, 2017, **739**, 439–446.
8 G. B. Nair and S. J. Dhoble, *J. Fluoresc.*, 2017, **27**, 575–585.
9 Z. M. Wang, J. Zou, C. Y. Zhang, M. M. Shi, B. B. Yang, Y. Li, H. Y. Zhou, Y. M. Liu, M. T. Li and X. L. Qian, *J. Mater. Sci.: Mater. Electron.*, 2018, **29**, 8767–8773.
10 J. S. Mao, H. W. Fang and Y. H. Chen, *J. Rare Earths*, 2018, **36**, 1157–1161.
11 D. Zhao, S. R. Zhang, R. J. Zhang, B. Z. Liu and Q. X. Yao, *Chem. Eng. J.*, 2021, **428**, 131023.
12 A. J. José, S. Mariana and M. Matthew, *Opt. Mater.*, 2020, **109**, 110336.
13 J. McKittrick, R. Shea, E. Lauren and D. J. Green, *J. Am. Ceram. Soc.*, 2014, **97**, 1327–1352.
14 G. Y. Lee, J. Y. Han, W. B. Im, S. H. Cheong and D. Y. Jeon, *Inorg. Chem.*, 2012, **51**, 10688–10694.
15 X. L. Gao, F. Song, A. Khan, Z. Y. Chen, D. D. Ju, X. Sang, M. Feng and L. S. Liu, *J. Lumin.*, 2020, 117707.
16 X. Yang, J. C. Chen, C. F. Chai, S. S. Zheng and C. Chen, *Optik*, 2019, **198**, 163238.
17 G. B. Naira, A. Kumara, S. J. Dhobleb and H. C. Swarta, *Mater. Res. Bull.*, 2020, **122**, 110644.
18 E. Hagar, O. Hosam, H. Ibrahim, I. Medhat and D. L. Dominique, *Materials*, 2019, **12**, 4140.
19 J. M. Millet, H. S. Parker and R. S. Roth, *J. Am. Ceram. Soc.*, 1986, **69**, 103–105.
20 B. M. Gatehouse, S. N. Platts and R. S. Roth, *Acta Crystallogr., Sect. C: Cryst. Struct. Commun.*, 1991, **47**, 2285–2287.
21 J. Bennazha, A. Boukhari and E. M. Holt, *Acta Crystallogr., Sect. C: Cryst. Struct. Commun.*, 2002, **58**, i29–i30.
22 J. C. Zhang, Y. Z. Long, H. D. Zhang, B. Sun, W. P. Han and X. Y. Sun, *J. Mater. Chem*, 2014, **2**, 312–318.
23 H. J. Guo, W. B. Chen, W. Zeng, Y. H. Wang and Y. Y. Li, *ECS Solid State Lett.*, 2015, **4**, R1–R3.
24 Y. Y. Li, W. B. Chen and Y. H. Wang, *Mater. Res. Bull.*, 2016, **84**, 363–369.
25 Z. C. Wu, Z. M. Zhang, C. Huang, J. Liu, M. M. Wu and Z. G. Xia, *J. Alloy Compd.*, 2017, **734**, 43–47.
26 Z. C. Wu, L. L. Cui, X. Zhang, X. X. Zhang, J. Liu, L. Ma, X. J. Wang and J. L. Zhang, *J. Alloy Compd.*, 2020, **835**, 155109.
27 D. Peng and S. Y. Jae, *Appl. Phys. A*, 2019, **125**, 101.
28 M. Yan, D. C. Zhu, Y. Pu and Q. Yan, *Optik*, 2021, **229**, 166250.
29 G. Blasse, *Phys. Lett.*, 1968, **28**, 444–445.
30 R. D. Shannon, *Acta Cryst.*, 1976, **32**, 751–767.
31 M. Y. Peng, Z. W. Pei, G. Y. Hong and Q. Su, *J. Mater. Chem.*, 2003, **13**, 1202–1205.